Critical behavior study of magnetic transitions in Dy_3Co single crystals

A. Herrero [a], A.Oleaga [a, *], A Salazar [a], A. F. Gubkin [b, c], N. V. Baranov [b, c]

[a] Departamento de Física Aplicada I, Escuela de Ingeniería de Bilbao, Universidad del País Vasco UPV/EHU, Plaza Torres Quevedo 1, 48013 Bilbao, Spain
[b]M.N. Miheev Institute of Metal Physics, Ural Branch of the Russian Academy of Sciences, 620108 Ekaterinburg, Russia
[c]Institute of Natural Sciences and Mathematics, Ural Federal University, 620083 Ekaterinburg, Russia

[*]Corresponding author: Departamento de Física Aplicada I, Escuela de Ingeniería de Bilbao, Universidad del País Vasco UPV/EHU, Plaza Torres Quevedo 1, 48013 Bilbao, Spain. Phone +34946014008. E-mail: alberto.oleaga@ehu.es

Abstract

An *ac* photopyroelectric calorimeter has been used to study the critical behaviour of the magnetic transitions in Dy_3Co measuring thermal diffusivity, specific heat and thermal conductivity, at low temperature. There are two phase transitions, both of which present singularities in the three variables. The antiferromagnetic to paramagnetic phase transition at ≈ 42 K complies with the short range, isotropic universality class, 3D-Heisenberg (α_{exp} = -0.133 for specific heat, b_{exp} = -0.145 for thermal diffusivity, α_{theor} = b_{theor} = -0.13). In the case of the lower transition where there is a rearrangement of the antiferromagnetic spin ordering at ≈ 32 K the critical behavior shows a deviation from isotropy. These results are linked to magnetic measurements already found in literature.

Keywords: Critical behavior; R_3Co; universality class; Photopyroelectric calorimeter; spin-ordering

1. Introduction

The intermetallic family R_3T (*R*=Gd, Tb, Dy, Ho, Er; *T*=Co, Ni) is specially interesting because of its promising technological applications: in the first place they are potential cryocoolers due to the presence of an important magnetocaloric effect; besides, they also present giant magnetoresistance as well as relatively high spin-ordering temperatures for the rare earths [1]. In order to explore the possible capabilities and

applications, a knowledge as deep as possible of the physical properties of the system is necessary, including the details of the phase transitions, such as the ordering of the spins, the extent of the interaction (short or long range order), etc.

The spin ordering in rare earths has traditionally been explained by means of the RKKY (Ruderman–Kittel–Kasuya–Yosida) interaction, which consists of an indirect exchange interaction between 4f-4f electron spins by means of conduction electron spins. But this description has been found not to be adequate for rare earth in metals, where it presents significant shortcomings [2]. Along the last 30 years a more complete picture has been developed to account for the magnetic interactions in rare earth in metals and, in particular, in R_3Co.

Though it could be expected, at first, to have two spin-ordering transitions in R_3Co (one corresponding to the 3d electron spins for the transition metal Co and another one for the 4f spins of the rare earth *R*), there is no ordering of the Co spins. Several exchange interactions take part in the magnetic ordering in rare earth (*R*)–3d transition metal (*T*) compounds [2-5]. The first process involved is the polarization of 5d spin moments parallel to the 4f moments, which takes place in *R* ions with a non-filled 4f electron shell, due to a 4f-5d intra-atomic exchange. This kind of polarization has already been experimentally observed in *R*-*T* compounds [6]. Furthermore, as it is well known, the increase of the rare earth atomic number contracts the 4f shell reducing the overlap between this and the 5d shell. This fact implies a decrease on the 4f-5d exchange energy for increasing atomic numbers of *R*.

A second type of mechanism is caused by the hybridization effects between 5d and 3d electrons and their short-range exchange and, as a consequence, 4f and 3d spins align themselves in antiparallel orientation, which is known as the f-d exchange interaction.

After presenting these mechanisms, we can go on describing the most accepted model for the indirect 4f-4f coupling in pure rare earths, with the aim of understanding the R_nT_m compounds. In the model introduced by Campbell [2] (which is valid for pure *R* compounds), the 4f-4f coupling consists of two steps: an intra-atomic 4f-5d exchange followed by an inter-atomic 5d-5d spin interaction between neighbouring R atoms, leading to a 4f-5d-5d-4f interaction. This mechanism also arises in R_nT_m compounds, but when these binary elements have a high rare earth content, the previous mechanism comes together with a 4f–5d–3d–5d–4f process. Therefore, R_nT_m compounds show different behaviour, regarding their magnetic ordering, depending on the *n:m* ratio. If this ratio is

small, the transition metal ions can have a net moment irrespective of the magnetic state of the rare earth sublattice. As the *n:m* ratio increases there is a decrease in the magnetic moment of the transition metals ions due to the filling of the 3d band on *T* atoms by outer-shell electrons of *R* atoms [7-9]. In particular, within the *R*-Co series, it has been found that, if the *R* atomic concentration is higher than 1/3, the magnetic moment of Co is lost.

Different studies have been undertaken to study the particulars of the magnetic ordering of the rare earth spins in R_3Co with *R* = Gd [10-15], Tb [16-18], Dy [19-22], Ho [23], and Er [24-25]. A shared feature among all of them is that there is an antiferromagnetic ordering from the paramagnetic phase, with T_N lowering as the atomic number increases. All of them have an orthorhombic crystal structure of the Fe_3C type (space group *Pnma*) where the rare earth occupies two non-equivalent positions: 4c (site symmetry m) and 8d (site symmetry I). The low symmetry orthorhombic crystalline structure in which *R* atoms occupy these two nonequivalent sites leads to an increase in crystal field effects. According to neutron diffraction studies [26], the magnetic structure of Tb_3Ni is non-coplanar owing to the competition between the influence of the low symmetry crystal electric field and the RKKY-exchange interaction described above. This complicated arrangement has been confirmed for Gd_3Co [11], Tb_3Co [18], Dy_3Co [19], Er_3Co [25], and Ho_3Co [23] with particularities depending on the rare earth atom. In the particular case of Dy_3Co, after the antiferromagnetic phase transition at about 42 K, there is a reorientation of the antiferromagnetic structure at about 32 K whose period has been suggested to be doubled along the *a*- and *c*- axes [19]. Another interesting feature in Dy_3Co is that it is suggested that there might exist a survival of short-range magnetic correlations in the paramagnetic state [20], as well as it happens in some other R_3(Co;Ni) compounds [27].

The aim of this paper is to study in detail the critical behavior of the two magnetic transitions in Dy_3Co associated with changes in spin orderings. Critical behavior theory assesses that a certain number of physical variables present anomalies in the near vicinity of the critical temperature T_C of a continuous phase transition, governed by a series of critical exponents, whose values are grouped in universality classes [28]. For example, the anomalies in specific heat and spontaneous magnetization can be written in that region, as a function of the reduced temperature $t = (T–T_C)/T_C$, as:

$$c_p(T) \sim A^{\pm} |t|^{-\alpha} \quad (A^- \text{ for } T < T_C,\ A^+ \text{ for } T > T_C) \tag{1}$$

$$M_S(T) \sim |t|^{\beta} \quad (T < T_C), \tag{2}$$

where α, β, A^+, A^- are the critical exponents and coefficients, whose values have been theorized by renormalization group theory for each universality class, on the basis of a particular Hamiltonian used as a starting point, which takes into account particular mechanisms and interactions to describe the phase transition. The exponents are universal in the sense that magnetic phase transitions in materials which are very different will be described by the same set of critical exponents, thus belonging to the same universality class. Table 1 shows the values of these exponents and coefficients for the most common magnetic universality classes [29-33]. This kind of study gives a clear insight in the underlying physics of a phase transition.

We will focus this work on the study of the critical behavior of the magnetic transitions in Dy_3Co using thermal variables: specific heat, thermal diffusivity and thermal conductivity. The main advantage of the thermal variables is that the critical exponents for the different universality classes are much more different among them (with even changes in sign) than what happens in the case of the magnetic exponents, where the differences are smaller (see Table 1).

2. Samples and experimental techniques

Dy_3Co polycrystalline samples were prepared by arc melting in a helium atmosphere using Dy and Co of 99.9% and 99.99% purity, respectively. The single crystal sample with dimensions of approximately 4 × 4 × 5 mm3 was grown by remelting the ingots at temperatures just above the peritecticpoint in a resistance furnace with a high temperature gradient, followed by annealing at 900 K for 3 days. The quality of the as-grown single crystal sample was characterized by the back reflection Laue method measuring x-ray diffraction patterns from different surfaces of the sample. No extra reflections from other grains were detected. Then the single crystal sample was cut into the plane-parallel slabs that are parallel to the (010) crystallographic plane. Those surfaces had been well polished and additionally checked by the back Laue method. The thicknesses of the slabs was about 600 μm.

A high-resolution *ac* photopyroelectric calorimetry in the back detection configuration has been used in this work to extract thermal diffusivity *D*, specific heat c_p and thermal conductivity *K*. This technique is particularly fitted to study phase transitions

in detail as a small temperature gradient in the sample gives rise to a high signal-to-noise ratio in the detector, obtaining the precise shape of the transitions in the close vicinity of the critical temperature with great resolution and a small uncertainty [34]. This technique has been extensively used to this end both with solid materials (to study magnetic as well as ferroelectric transitions) [35-41] and liquid crystals [42, 43].

The details of the experimental setup, measurement procedure, and the theory which explains how to retrieve thermal diffusivity, specific heat and thermal conductivity from the photopyroelectric signal can be found elsewhere [34, 40]. The slowest cooling and heating rates used for the high-resolution runs close to the transition temperatures have been about 20 mK/min.

3. Experimental Results

Fig. 1a presents the thermal diffusivity as a function of temperature in the region of interest. It is worth mentioning that at room temperature, the thermal diffusivity is 2.65 mm^2/s and it decreases with temperature till it reaches the value of 1.16 mm^2/s at 100 K, a behaviour quite typical of intermetallic materials due to the added contribution of the electronic and phononic part of the thermal diffusivity; below 100 K the phonon contribution starts to dominate, making the thermal diffusivity increase till 1.21 mm^2/s at 50K. From then on, the thermal diffusivity background quickly increases as the phonon mean free path is severely reduced and the magnetic transitions are superimposed on this background as two dips, as it has been found in many other materials [35-37, 40-41]. In this particular case, the dips are located at 32.07 K and 41.57 K.

Fig. 1b shows the specific heat in the same temperature range as Fig. 1a while Fig. 1c shows the thermal conductivity. Specific heat and thermal conductivity are always noisier than thermal diffusivity using this technique, as the latter is obtained only using the phase of the photopyroelectric signal while for the former two both amplitude and phase are needed. The position of the specific heat peaks (32.26 K and 41.82 K.) are similar to those found in literature [19], where it is firmly established that the transition at higher temperature corresponds to an antiferromagnetic ordering of the rare earth spins

from a paramagnetic state while the one at lower temperature is due to a reordering of those spins into another antiferromagnetic distribution. The thermal conductivity also presents singularities at both transitions; this magnitude has not been measured before in this intermetallic family. It is not usual to find anomalies in the form of peaks at magnetic transitions but it has been found for several magnetic transitions in materials such as Gd [35], FeF_2 [36], $RbMnF_3$ [37], and $KMnF_3$ [44]. The decreasing background in thermal conductivity with decreasing temperature is also another feature common to many intermetallic families [45-47].

4. Fitting procedure and discussion

The equation used to fit the experimental specific heat curves is:

$$c_p = B + Ct + A^{\pm}|t|^{-\alpha}\left(1 + E^{\pm}|t|^{0.5}\right) \quad , \tag{3}$$

where $t = (T - T_N)/T_N$ is the reduced temperature, T_N the critical temperature, and α, $A^{\pm}$, B, C and $E^{\pm}$ are adjustable parameters. Superscripts + and - stand for $T > T_N$ and $T < T_N$ respectively. The linear term represents the background contribution to the specific heat, while the last term is the anomalous contribution to the specific heat. The factor under parenthesis is the correction to scaling that represents a singular contribution to the leading power as known from experiments and theory [48, 49]. A simultaneous fit to both branches ($T > T_N$ and $T < T_N$) has been undertaken using a non-linear least square routine using a Levenberg-Marquardt method. The details of the fitting procedure can be found elsewhere [40].

Concerning thermal diffusivity, a similar equation to Eq. (3), used for specific heat, with its own critical parameters, is written as

$$D = V + Wt + U^{\pm}|t|^{-b}\left(1 + F^{\pm}|t|^{0.5}\right) \tag{4}$$

and an equivalent procedure to the one carried out with c_p has been followed.

The relations between the critical parameters of specific heat and thermal diffusivity are already studied for the most common magnetic universality classes: 3D-Heisenberg (isotropic distribution of spins), 3D-XY (easy plane anisotropy) and 3D-Ising (uniaxial anisotropy) [36, 37, 44, 50, 51]. In particular, in the Heisenberg case, the following relations can be written among the critical parameters [51]

$$b \approx \alpha, \tag{5a}$$

$$U^{+}/U^{-} \approx A^{+}/A^{-} \tag{5b}$$

In the case of thermal conductivity, the fitting is performed using its inverse, because all the thermal resistances associated to the various heat conduction mechanisms in the sample are in series:

$$1/K = 1/K_{nonmag} + 1/K_{mag} = L + Mt + N^{\pm}|t|^{-g}\left(1 + H^{\pm}|t|^{0.5}\right) \tag{6}$$

so that the singular term in Eq. (6) can be related to the magnetic contribution to the heat conduction processes. K_{nonmag} has to do with phonon-phonon scattering, umklapp, scattering with impurities, etc., while K_{mag} refers to the spin-phonon scattering mechanisms. The magnetic resistive term originates from the spin-lattice interaction and, close to T_N, from an additional term that accounts for phonon scattering by critical fluctuations of the order parameter.

Fig. 2 shows the fittings for the three magnitudes: thermal diffusivity, specific heat and the inverse of the thermal conductivity, for the paramagnetic to antiferromagnetic phase transition in the near vicinity of the Néel temperature as a function of the reduced temperature $t=(T-T_N)/T_N$, where the dots correspond to the experimental and the continuous lines to the best fitting to Eqs. (3), (4) and (6). The figure also contains the deviation plots of each fitting with respect to the experimental curves, assessing the quality of the fittings . Table 2 contains the values of the critical parameters together with the root mean square value ($R^2 = 1$ means a perfect fitting). If attention is focused on the results for specific heat, the critical parameters agree quite well with the isotropic 3D-Heisenberg model ($\alpha_{exp} = -0.133 \pm 0.014$, $A^{+}/A^{-}_{exp} = 1.64$, $\alpha_{theor} = -0.134$ [31], $A^{+}/A^{-}_{exp} = 1.52$ [33]). We would like to point out that the theoretical value for the critical parameter α in the 3D-Heisenberg universality class mainly used in literature

is -0.115 but the most recent calculations performed by Campostrini *et al.* [31] have increased this value to -0.134, which is precisely the value we have obtained in this transition.

The slight deviation between the experimental and the theoretical value of the critical ratio A^+/A^- might be attributed to a lack of complete isotropy, as manifested in the ac susceptibility measurements along the three axes [19], which shows some differences.

Our results confirm that both the critical exponent and the ratio of the critical coefficients for the thermal diffusivity nearly match those for specific heat, where b = -0.145±0.020, U^+/U^- = 1.41. Both parameters can be considered to fulfill the approximate Eqs. (5a) and (5b), confirming the adscription to the Heisenberg class. Finally, the inverse of the thermal conductivity also gives a close value of its critical exponent g to the Heisenberg model (-0.101) while the ratio of the critical coefficients N^+/N^- gets away from the theoretical value (0.94). This behavior for the inverse of thermal conductivity is very similar to the one found for other isotropic magnets such as $RbMnF_3$ (g = -0.08, N^+/N^- =1.1) [37] and $KMnF_3$ (g = -0.10, N^+/N^- =1.15) [44], although further studies are necessary in order to fully understand its meaning.

Another interesting conclusion is that, indeed, our results declare that short range order interactions are responsible for this magnetic transition and not long range ones (for which the proper universality class would have been the mean field model). This is in agreement with the studies which have pointed out that even in the paramagnetic phase there is a survival of short range order interactions [20], as it also happens in some other R_3(Co,Ni) [27].

Now we will turn our attention to the lower temperature transition, where the ordering changes from one antiferromagnetic structure to another one. Fig. 3 shows the equivalent to Fig. 2 for this transition and Table 3 displays the equivalent information to Table 2. The critical exponent for specific heat does not really comply with any universality class (α_{exp} = -0.168±0.009, A^+/A^-_{exp} = 1.18); there is a stronger deviation from the 3D-Heisenberg class but without reaching neither the 3D-XY (α_{theor} = -0.014, A^+/A^-_{exp} =1.06) nor the 3D-Ising (α_{theor} = 0.11, A^+/A^-_{exp} = 0.53). Our interpretation is that the isotropy is being smoothed somehow, in agreement with Baranov *et al* [21] who showed that there is a smaller projection of the magnetic moment along the *b*-axis than along the *a*- and *c*- axes (4.5 μ_B, 6.0 μ_B and 6.3 μ_B, respectively) [19,21], giving rise to what is labeled as “a highly anisotropic non-collinear magnetic structure” [21] but without the

presence of an easy plane or an easy axis. Magnetic susceptibility measurements have also assessed an important difference in the spin ordering in the two transitions: In the higher temperature one there is an anomaly in χ when applying magnetic field along the three axes *a*, *b* and *c* while in the lower temperature one the anomaly is only visible when applying the field along the *b*-axis [19, 22].

This deviation from an isotropic magnet is further confirmed with the fittings for thermal diffusivity (b = -0.139±0.020, U^+/U^- = 0.85) and the inverse of the thermal conductivity (g = -0.096, N^+/N^- = 0.98). The deviations in the fulfillment of Eqs. (5a) and (5b) are now strong, supporting that the Heisenberg class is no longer of application.

5. Conclusions

The critical behaviour of the two magnetic transitions that Dy_3Co presents at low temperature has been studied on the singularities that thermal diffusivity, specific heat and thermal conductivity show. The antiferromagnetic to paramagnetic phase transition at about 42 K is governed by short range interactions and belongs to the 3D-Heisenberg universality class, proved not only by the critical exponents for specific heat (α = -0.133) and thermal diffusivity (b = -0.145) but also by the relations between the parameters obtained in the fittings. In the case of the lower transition at about 32 K (change of antiferromagnetic ordering) there is a clear deviation from this isotropic class.

Acknowledgments

This work has been supported by Universidad del País Vasco/Euskal Herriko Unibertsitatea (UPV/EHU-GIU16/93) and also partially supported by FASO of Russia (themes No 01201463328 and 01201463334). The Laue x-ray diffraction measurements have been performed in the Center of Collaborative Access of IMP UB of RAS.

References

[1] X. Zheng, B. Shen, Chin. Phys. B 26 (2017) 027501.

[2] I. A. Campbell, J. Phys. F: Met. Phys. 2 **(**1972) L47.

[3] M. S. S. Brooks, L. Nordstrom, B. Johansson, Physica B 172 (1991) 95-100.

[4] D. Givord, D. J. Courtois, J. Magn. Magn. Mater. 196/197 (1999) 684-688.

[5] B. Johansson, L. Nordstrom, O. Eriksson, M. S. S. Brooks, Phys. Scr. T39 (1991) 100.

[6] N. H. Duc *Handbook on Physics and Chemistry of Rare Earths* vol 24, ed K A Gschneidner Jr and L Eyring (Amsterdam: Elsevier) chapter 163 (1997)

[7] N. H. Duc, P. E. Brommer, *Handbook of Magnetic Materials* vol 12, ed K. H. J. Buschow (Amsterdam: Elsevier Science B.V.) chapter 3 (1999) 259-394.

[8] H. Kirchmayr, C. A. Poldy, *Handbook on Physics and Chemistry of Rare Earths* vol 2, ed K. A. Gschneidner Jr and L. Eyring (Amsterdam: North-Holland) chapter 14 (1979) 55-230.

[9] N. R. Taylor, Adv. Phys. 20 (1971) 551-660.

[10] S.K. Tripathy, K.G. Suresh, A.K. Nigam, J. Magn. Magn. Mat. 306 (2006) 24-29.

[11] N.V. Tristan, S.A. Nikitin, T. Palewski, and K. Skokov, J. Magn. Magn. Mat. 251 (2002), 148-154.

[12] N.V. Baranov, A.V. Andreev, A.I. Kozlov, G.M. Kvashnin, H. Nakotte, H. Aruga Katori, T. Goto, J. Alloys Compd. 202 (1993) 215-224

[13] N.V. Baranov, G. Hilscher, P.E Markin, H. Michor, A.A. Yermakov, J. Magn. Magn. Mater. 272-276 (2004) 637-638.

[14] N.V. Tristan, S.A. Nikitin, T. Palewski, K. Nenkov, and K. Skokov , J. Magn. Magn. Mater. 258 (2003) 583-585.

[15] N. V. Tristan, K. Nenkov, T. Palewski, K. P. Skokov, S. A. Nikitin, Phys. Stat. Sol. (a) 196 (2003) 325-328.

[16] N. V. Baranov, A.V Deryagin, A. I. Kozlov, Ye. V. Sinitsyn, Phys. Met. Metall. 61 (1986), 97-106.

[17] B. Li, J. Du, W. J. Ren, W. J. Hu, Q. Zhang, D. Li, Z. D. Zhang, Appl. Phys. Let. 92, (2008) 242504.

[18] N. V. Baranov, A. F. Gubkin, A. P. Vokhmyanin, A. N. Pirogov, A. Podlesnyak, L. Keller, N. V. Mushnikov and M. I. Bartashevich, J. Phys.: Condens. Matter 19 (2007) 326213.

[19] N.V. Baranov, A.N. Pirogov, A.E. Teplykh , J. Alloys Compd. 226 (1995) 70-74.

[20] J. Shen, J. L. Zhao, F.X. Hu, G. H. Rao, G. Y. Liu, J. F. Wu, Y. X. Li, J. R. Sun, B. G. Shen, Appl Phys A, 99 (2010) 853-858.

[21] N.V. Baranov, E. Bauer, R. Hauser, A. Galatanu, Y. Aoki, H. Sato, Eur. Phys. J. B 16 (2000) 67-72.

[22] P. Svoboda, H. Nakotte, A. M. Alsmadi, M. Doerr, Acta Physica Polonica B 34, (2003) 1449.

[23] N. V. Baranov, T. Goto, G. Hilscher, P. E. Markin, H. Michor, N. V.Mushnikov, J-G Park, A. A. Yermakov, J. Phys.: Condens. Matter 17 (2005) 3445.

[24] P. Kumar, N.K. Singh, A.K. Nayak, A.Haldar, K. G. Suresh, A. K. Nigam, J. of App. Phys. 107 (2010) 09A932.

[25] A. F. Gubkin, A. Podlesnyak, N. V. Baranov, Phys. Rev. B 82 (2010) 012403.

[26] D. Gignoux, J. C. Gomezsal, D. Paccard, Solid State Comm. 44 (1982) 695.

[27] N.V. Baranov, A.V.Proshkin, A.F.Gubkin, A.Cervellino, H.Michor, G.Hilscher, E.G. Gerasimov, G.Ehlers, M.Frontzek, A.Podlesnyak, J. Magn. Magn. Mat. 324 (2012) 1907-1912.

[28] H. E. Stanley, "Introduction to phase transitions and critical phenomena", Oxford University Press (1971).

[29] R. Guida, J. Zinn-Justin J, J. Phys. A: Math Gen. 31 (1998) 8103.

[30] M. Campostrini, M. Hasenbusch, A. Pelisseto, P. Rossi, and E. Vicari, Phys. Rev. B 63 (2001) 214503.

[31] M. Campostrini, M. Hasenbusch, A. Pelisseto, P. Rossi, and E. Vicari, Phys. Rev. B 65 (2002) 144520.

[32] M. Hasenbusch, Phys. Rev. B 82 (2010) 174434.

[33] C. Bervillier, Pyhs. Rev. B 34, 8141 (1986).

[34] U. Zammit, M. Marinelli, F. Mercuri, S. Paoloni, F. Scudieri, Rev. Scient. Inst. 82 (2011) 121101.

[35] C. Glorieux, J. Thoen, G. Bednarz, M.A. White, D.J.W. Geldart, Phys. Rev. B 52, (1995) 12770.

[36] M. Marinelli, F. Mercuri, D.P. Belanger, Phys. Rev. B 51 (1995) 8897.

[37] M. Marinelli, F. Mercuri, S. Foglietta, D.P. Belanger, Phys. Rev. B 54 (1996) 4087.

[38] M. Massot, A. Oleaga, A. Salazar, D. Prabhakaran, M. martin, P. Berthet, G. Dhalenne, Phys. Rev. B 77 (2008) 134438.

[39] A. Oleaga, A. Salazar, D. Prabhakaran, J.G. Cheng , J.S. Zhou, Phys. Rev. B 85 (2012) 184425.

[40] A. Oleaga, V. Shvalya, A. Salazar, I. Stoika, Yu. M. Vysochanskii, J. Alloys Compd. 694 (2017) 808-814.
[41] A. Oleaga, A. Salazar, D. Skrzypek, J. Alloys Compd. 629 (2015) 178-183.
[42] U. Zammit, S. Paoloni, F. Mercuri, M. Marinelli, F. Scudieri, AIP Adv. 2 (2012) 012135.
[43] U. Zammit, F. Mercuri, S. Paoloni, M. Marinelli, R. Pizzoferrato, J. Appl. Phys. 117 (2015) 105104.
[44] A. Salazar,M. Massot, A. Oleaga, A. Pawlak, W. Schranz, Phys. Rev. B 75 (2007) 224428.
[45] A. Kowalczyk, M. Falkowski, Intermetallics 37 (2013) 65-68.
[46] M. Wencka, M. Hahne, A. Kocjan, S. Vrtnik, P. Kozelj, D. Korze, Z. Jaglicic, M. Soric, 1, P. Popcevic, J. Ivkov, A. Smontara, P. Gille, S. Jurga, P. Tomes, S. Paschen, A. Ormeci, M. Armbrüster, Yu. Grin, J. Dolinsek, Intermetallics 55 (2014) 56-65.
[47] A. K. Bashir, M. B.T. Tchokonté, A.M. Strydom, J. Magn. Magn. Mat. 414 (2016) 69-73.
[48] M. Marinelli, F. Mercuri, U. Zammit, R. Pizzoferrato, F. Scudieri, D. Dadarlat, Phys. Rev. B 49 (1994) 9523.
[49] A. Kornblit, G. Ahlers, Phys. Rev. B 11 (1975) 2678.
[50] A. Oleaga, A.Salazar, Yu.M. Bunkov, J.Phys.: Condens. Matter 26 (2014) 096001.
[51] A. Pawlak, Phys. Rev. B 68, 094416 (2003)

Table 1. Most common magnetic universality classes in three dimensions and the corresponding critical parameters. α and A^+/A^- are for specific heat, β for spontaneous magnetization, γ for isothermal susceptibility [29-33].

Universality class	Interaction Range	Spin symmetry	α	β	γ	A^+/A^-
3D-Ising	Short range	Uniaxial anisotropy	0.11	0.33	1.24	0.52
3D-XY	Short range	Easy plane anisotropy	-0.014	0.34	1.30	1.06
3D-Heisenberg	Short range	Isotropic	-0.13	0.36	1.39	1.52
Mean Field Model	Long range		0	0.5	1	--

Table 2. Critical parameters and quality of the fittings (given by the root mean square value) for the antiferromagnetic to paramagnetic transition in Dy_3Co

	α	**A^+/A^-**	**T_N(K)**	**A^+ ($Jkg^{-1}K^{-1}$)**	**B ($Jkg^{-1}K^{-1}$)**	**C ($Jkg^{-1}K^{-1}$)**	**E^+ ($Jkg^{-1}K^{-1}$)**	**E^- ($Jkg^{-1}K^{-1}$)**	**R^2**
c_P ($Jkg^{-1}K^{-1}$)	-0.133±0.014	1.64	42.24	-160±3	208±7	331±9	-0.48±0.09	-0.56±0.02	0.99852
	b	**U^+/U^-**	**T_N(K)**	**U^+ (mm^2/s)**	**V (mm^2/s)**	**W (mm^2/s)**	**F^+ (mm^2/s)**	**F^- (mm^2/s)**	**R^2**
D (mm^2/s)	-0.145±0.020	1.41	41.96	0.95±0.01	0.83±0.05	-2.08±0.07	-0.16±0.10	-0.999±0.078	0.99103
	g	**N^+/N^-**	**T_N(K)**	**N^+ (Km/W)**	**L (Km/W)**	**M (Km/W)**	**H^+ (Km/W)**	**H^- (Km/W)**	**R^2**
1/K (Km/W)	-0.101±0.009	0.94	42.14	0.54±0.03	0.31±0.03	-2.23±0.05	0.71±0.08	-1.9±0.2	0.99504

Table 3. Critical parameters and quality of the fittings (given by the root mean square value) for the antiferromagnetic to antiferromagnetic transition in Dy_3Co

	α	**A^+/A^-**	**T_N(K)**	**A^+ ($Jkg^{-1}K^{-1}$)**	**B ($Jkg^{-1}K^{-1}$)**	**C ($Jkg^{-1}K^{-1}$)**	**E^+ ($Jkg^{-1}K^{-1}$)**	**E^- ($Jkg^{-1}K^{-1}$)**	**R^2**
c_P ($Jkg^{-1}K^{-1}$)	-0.168±0.009	1.18	32.38	-204±2	183±4	458±7	-0.24±0.03	-1.49±0.07	0.99622
	b	**U^+/U^-**	**T_N(K)**	**U^+ (mm^2/s)**	**V (mm^2/s)**	**W (mm^2/s)**	**F^+ (mm^2/s)**	**F^- (mm^2/s)**	**R^2**
D (mm^2/s)	-0.139±0.033	0.85	32.10	2.1±0.2	0.3±0.3	-8.9±0.7	1.1±0.3	-2.3±0.5	0.99652
	g	**N^+/N^-**	**T_N(K)**	**N^+ (Km/W)**	**L (Km/W)**	**M (Km/W)**	**H^+ (Km/W)**	**H^- (Km/W)**	**R^2**
1/K (Km/W)	-0.096±0.020	0.99	32.44	1.03±0.12	0.1±0.1	-2.78±0.09	0.21±0.05	-1.3±0.2	0.99807

Figure Captions

Fig. 1. Thermal diffusivity (D), specific heat (c_p) and thermal conductivity (K) as a function of temperature for Dy_3Co.

Fig. 2. Experimental (dots) and fitted curves (continuous lines) of the specific heat (a), thermal diffusivity (c) and inverse of thermal conductivity (e) as a function of the reduced temperature for the antiferromagnetic to paramagnetic transition in Dy_3Co. (b), (d), and (f) present the corresponding deviation plots. Open circles are for $T < T_N$ and crosses for $T > T_N$.

Fig. 3. Experimental (dots) and fitted curves (continuous lines) of the specific heat (a), thermal diffusivity (c) and inverse of thermal conductivity (e) as a function of the reduced temperature for the antiferromagnetic to antiferromagnetic transition in Dy_3Co. (b), (d), and (f) present the corresponding deviation plots. Open circles are for $T < T_N$ and crosses for $T > T_N$.

Fig. 1

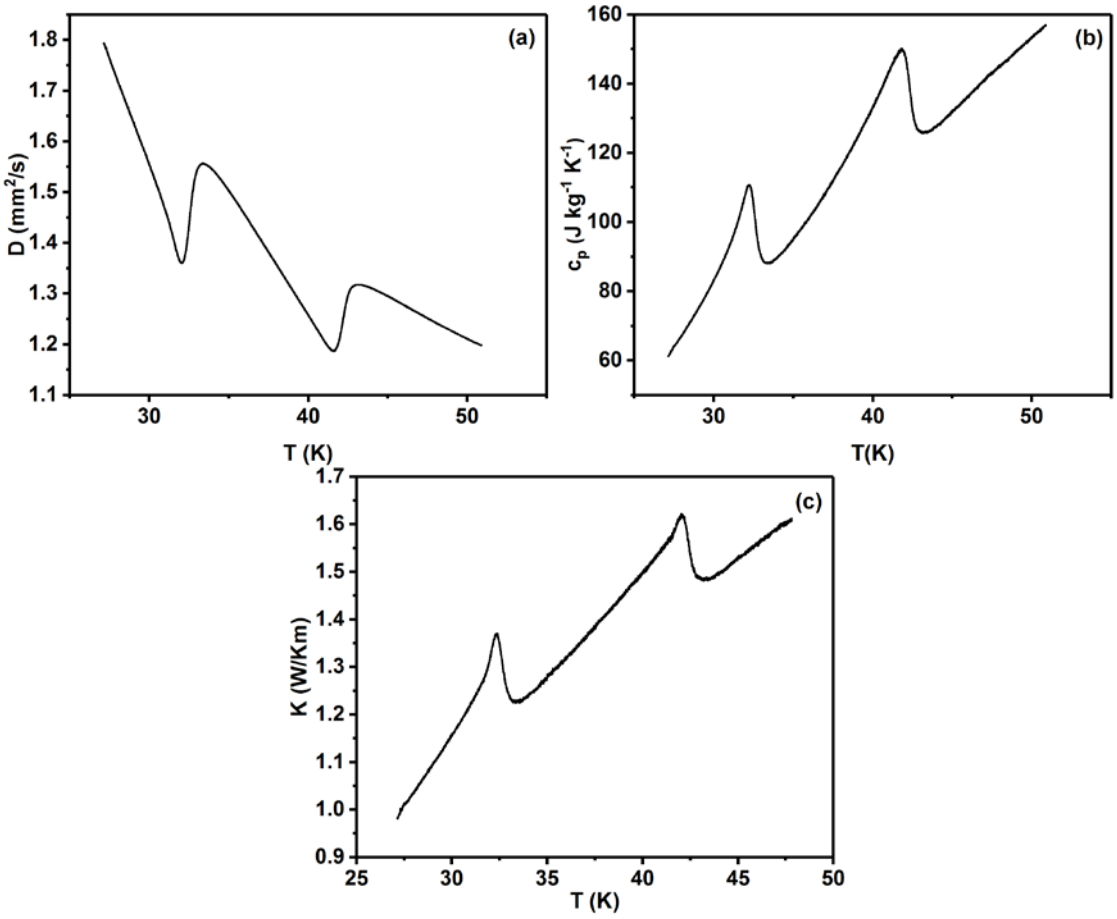

Fig. 2

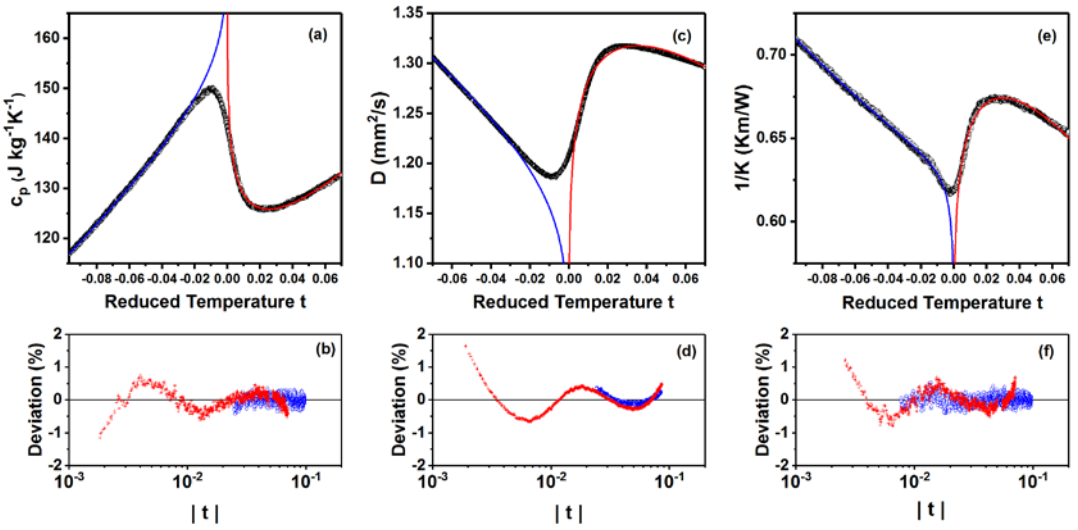
(a)
(b)
(c)
(d)
(e)
(f)
c_p (J kg^{-1}K^{-1})
D (mm^2/s)
1/K (Km/W)
Deviation (%)
Reduced Temperature t
| t |

Fig. 3

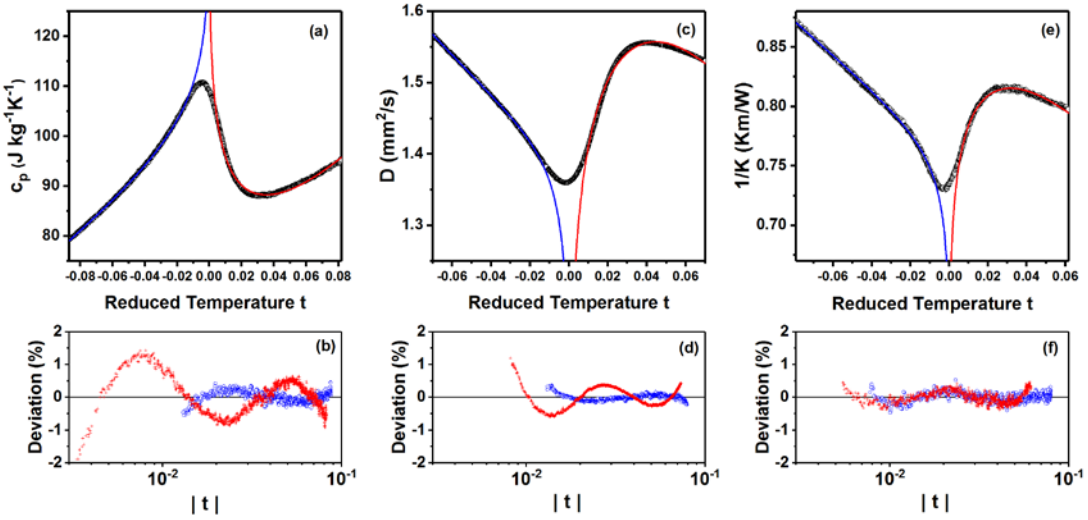
(a)
(b)
(c)
(d)
(e)
(f)
c_p (J kg^{-1}K^{-1})
D (mm^2/s)
1/K (Km/W)
Deviation (%)
Reduced Temperature t
| t |